Available online at www.sciencedirect.com

ScienceDirect

Procedia Structural Integrity 24 (2019) 190–203

Structural Integrity Procedia

www.elsevier.com/locate/procedia

AIAS 2019 International Conference on Stress Analysis

Fatigue properties of austempered ductile iron-to-steel dissimilar arc-welded joints

Giovanni Meneghetti[a]*, Alberto Campagnolo[a], Daniele Berto[a], Elena Pullin[a], Stefano Masaggia[b]

[a] *Department of Industrial Engineering, University of Padova, Via Venezia, 1 – 35131 Padova (Italy)*

[b] *Zanardi Fonderie Spa, Via Nazionale 3, 37046 Minerbe (Verona - Italy)*

Abstract

The structural design of mechanical systems increasingly leads to the adoption of different materials in order to improve the performance of a structure. A possible solution is the adoption of dissimilar arc-welded joints, which often must be able to withstand high cyclic loads under service conditions. Being a recently available joining technology, the design standards and recommendations do not report fatigue strength categories for dissimilar joints, therefore dedicated investigations are necessary. In the present contribution, the fatigue behavior of EN-JS-1050 austempered ductile iron-to- S355J2 steel dissimilar arc-welded joints has been experimentally investigated to determine the fatigue strength categories of some typical welded details and to compare them with the categories provided by standards and recommendations for homogeneous welded steel joints. First, dissimilar joints were evaluated by metallographic analysis, then micro-hardness profiles were measured. Experimental fatigue tests were performed on (i) partially-penetrated butt-joints and fully-penetrated ground butt joints under axial loading and (ii) fully-penetrated butt joints and cruciform non-load-carrying fillet-welded joints under four-point bending loading. All joints were in the as-welded conditions. The fracture surfaces of the joints were analyzed to identify fatigue crack initiation locations.

Keywords: dissimilar welded joints; austempered ductile iron; structural steel; fatigue behaviour.

* Corresponding author. Tel.: 0039 049 827675; fax: 0039 049 8276785.
E-mail address: giovanni.meneghetti@unipd.it

10.1016/j.prostr.2020.02.016

1. Introduction

In several industries, the structural design of mechanical systems increasingly leads to the combination of various materials into a multi-material structure. The different properties of the adopted materials are jointly employed to obtain high performance structures and to integrate an increased number of functions. However, joining together materials having different chemical, mechanical, thermal, or electrical properties brings also significant challenges. The potential incompatibility, in terms of thermal expansion, ductility, fatigue strength, elastic modulus etc, could adversely affect the joining process itself, but also the structural integrity of the joints during in-service conditions. Martinsen et al. (2015) have recently reviewed advantages and challenges of joining dissimilar materials.

Structural components made of dissimilar materials can be joined together by welding. In the relevant literature, several contributions have been devoted to investigate the possibility of joining dissimilar materials by different welding techniques: the most widely adopted is the friction-welding (Okamura and Aota (2004); Uzun et al. (2005); Figner et al. (2009); Taban et al. (2010); Paventhan et al. (2011); Mohammadzadeh Polami et al. (2015); Infante et al. (2016); Eslami et al. (2019)), but also arc-welding (Roberts et al. (1985); Bettahar et al. (2015); Zhang et al. (2016); Kumar et al. (2017); Zhang et al. (2018b); Zhang et al. (2018a); Al Zamzami et al. (2019)), laser-welding (Katayama (2004); Parkes et al. (2013)) and other techniques, such as resistance spot welding (Sun et al. (2017); Rao et al. (2018)) and magnetic pulse welding (Geng et al. (2019)) are employed. In the context of arc-welding, Austempered Ductile Iron (ADI) to structural steel dissimilar joints offer the possibility to improve mechanical response of structural components, combining weight reduction and net-to-shape geometry at the same time. Indeed, the possibility for iron castings to be designed with complex shape and low thickness, together with the very good static, impact, fatigue performances and moderate wear resistance offered by ADI, allows the optimization of mass distribution based on both actual stiffness and required load levels. Thus, the use of steel can be limited where needed or mandatory.

Dissimilar welded joints must also be able to withstand high cyclic loads under service conditions. Concerning the design of welded joints against fatigue loading, different approaches are available in International Standards and Recommendations (Eurocode 3 (2005); Eurocode 9 (2011); Hobbacher (2016)), namely the nominal stress, the hot-spot stress, the notch stress and the Linear Elastic Fracture Mechanics (LEFM) approaches. The nominal stress approach is based on stress calculations according to solid mechanics and it is the easiest and most widely adopted. Essentially, the fatigue strength assessment of a welded structure is performed by comparing the calculated nominal stress with the proper design category of the joint, which primarily depends on the considered geometry and loading condition. However, International Standards and Recommendations (Eurocode 3 (2005); Eurocode 9 (2011); Hobbacher (2016)) provide fatigue strength categories to apply the nominal stress approach only to homogeneous welded joints made of structural steels or aluminum alloys and not for dissimilar joints. Several contributions in the recent literature have addressed the analysis of the fatigue behavior of dissimilar joints made of different grades of structural steels (Roberts et al. (1985); Paventhan et al. (2011); Parkes et al. (2013); Bettahar et al. (2015); Mohammadzadeh Polami et al. (2015); Zhang et al. (2016); Kumar et al. (2017); Zhang et al. (2018b); Zhang et al. (2018a)), different series of aluminum alloys (Infante et al. (2016)), a steel and an aluminum alloy (Okamura and Aota (2004); Uzun et al. (2005); Figner et al. (2009); Taban et al. (2010)) or other metallic materials welded together (Sun et al. (2017); Eslami et al. (2019)). However, to the best of Authors' knowledge, in the relevant literature there is no contribution which has investigated the fatigue behavior of dissimilar arc-welded joints made of ADI and structural steel. Due to the lack of information in the technical literature and in all International Standards and Recommendations (Eurocode 3 (2005); Hobbacher (2016)), the fatigue behavior of austempered ductile iron (EN-JS-1050)-to-steel (S355J2) dissimilar arc-welded joints has been experimentally investigated in the present contribution. Afterwards, the aims of the present contribution are:

- to evaluate the microstructure of post-weld materials in ADI-steel joints by metallographic analysis and to measure micro-hardness profiles;
- to perform experimental fatigue tests on ADI-steel joints considering some typical welded details and to analyze the fracture surfaces of the joints to identify the fatigue crack initiation locations;
- to derive the fatigue strength categories of the tested welded details and to compare them with the categories provided by standards and recommendations for homogeneous welded steel joints.

2. Testing program

S355J2 EN10025-2 hot rolled construction steel (S355J2) is commonly used for structural applications, while ISO 17804 JS/1050-6 Austempered Ductile Iron (ADI 1050) for earth movement undercarriage components, suspension parts, axles, power transmission components, etc.

ADI 1050 is produced by heat-treating a low alloyed Pearlitic-Ferritic Ductile Iron, cast after a special preconditioning of the metal bath. The cast material is made of iron where carbon is mainly present in the form of spheroidal graphite particles. The isothermal heat treatment of spheroidal graphite cast iron, known as "Austempering", basically consists in:

- heating the castings at 900°C;
- cooling in salt bath having constant temperature of 350 °C, at a cooling rate able to promote the formation of "Ausferrite".

This process produces a microstructure that consists predominantly of retained austenite and acicular ferrite. The new matrix is called "Ausferritic" and gives to the new material unique mechanical properties, comparable to a 42CrMo4Q&T steel material.

The fatigue tested joint geometries are reported in Fig. 1 along with details about the loading conditions, the testing conditions being described in more detail in next Section 5 and Table 3.

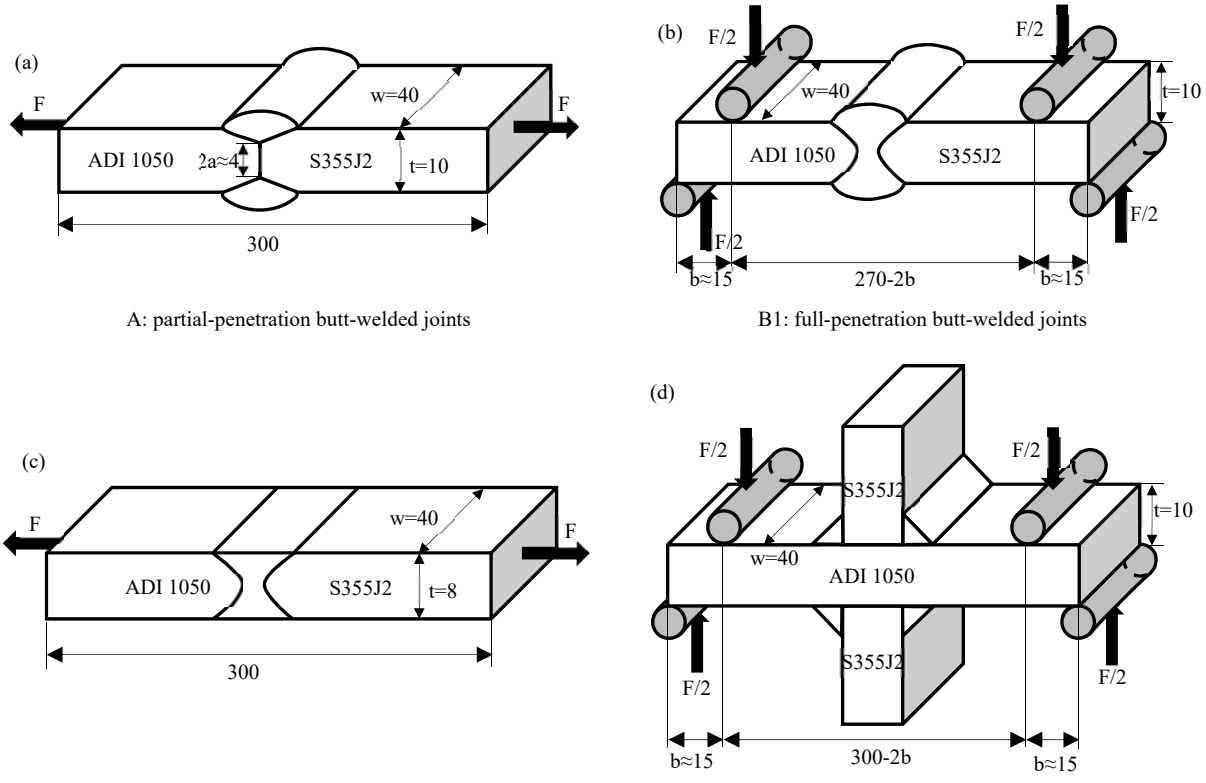

A: partial-penetration butt-welded joints

B1: full-penetration butt-welded joints

B2: full-penetration ground butt-joints

C: cruciform non-load-carrying fillet-welded joints

Fig. 1. Geometries and loading conditions of dissimilar welded joints tested under fatigue loading.

3. Preparation of welded specimens

All specimens were obtained from plates having dimensions 300x150x12 mm. Ductile iron plates were poured by Zanardi Fonderie S.p.A. in horizontal greensand moulds printed using a proper experimental pattern plate; they were sand cleaned after shakeout, austempered to material grade ADI 1050 and milled to the final thickness of 10 mm.

Steel plates, having same initial dimensions, were prepared from commercial hot rolled plates and then reduced to 10 mm thickness by milling.

All plates were grinded, brushed and properly clamped by means of tack welded fixture bracket in order to minimize welding distortions. Final specimen's dimensions were obtained by cutting after welding. All welding operations were done by 'Istituto Italiano della Saldatura' (IIS).

ADI 1050 showed ultimate strength R_m=1100 MPa, yield strength R_{p02}=920 MPa, Brinell hardness HBW=350÷380 and elongation at fracture A_5=8%; all mechanical properties were obtained from specimens cut from the plates. S355J2 mechanical properties according to EN10025-2 are ultimate strength $R_{m\ min}$=470 MPa, yield strength $R_{p02\ min}$=355 MPa, HBW=160÷180 and elongation at fracture $A_{5\ min}$=22%.

3.1 Production of specimens

Welding parameters were tuned (Meneghetti et al. (2019)) by considering the specimen's thickness of 10 mm, weld bead dimensions, misalignments, runs number and all the different types of dissimilar joint investigated. The main issue was to prevent martensite formation and cracks nucleation within HAZ of ADI 1050: the proper set of welding parameters was identified in such a way that the resulting hardness was as close as possible to the base ADI material. However, the formation of ledeburite layer close to the weld metal cannot be avoided as in this area ductile iron always undergoes metastable solidification after re-melting. The complete set of welding parameters is reported in Table 1. In particular, pulsed arc fully mechanized GMAW-welding process was adopted.

Table 2 summarizes the specimens' geometry and preparation. Macrographic/micrographic tests as well as VT, PT and HBW test were carried out on all specimens. Quality level for imperfections was according to ISO 5817-B.

Table 1. GMAW welding parameters adopted for specimens

Mode of metal transfer	Welding position	Torche angle direction	Filler material	Current& Polarity [A]	Voltage [V]	Travel speed [mm/min]	Heat input [kJ/mm]
P	UNI EN ISO 6947 PA	15° forehand	S C NiFe-2 EN ISO 1071 ø 1.2 mm	CCPI 120÷130	24÷25	220÷340	0.41÷0.71
Preheat temperature			EN 13916-TC 200°C				
Interpass temperature			EN 13916-TC 250°C				
Shielding			ISO 14175 M21 (Ar-CO_2 80-20), flow rate 16÷18 lt/min				

4. Specimen characterisation

For all specimens, micro-hardness and residual stress profiles, along with misalignments, were measured (Meneghetti et al. (2019)) in order to evaluate the conditions of post-weld materials in ADI-steel joints. However, for the sake of brevity, only hardness measurements are reported in the present contribution.

Vickers hardness HV0.5 profiles were measured in order to recognize microstructural alterations. The results are reported in Figs. 2-5 and confirm that heat affected zone of ADI 1050 mainly consists in graphite nodules in pearlitic matrix and ledeburite layer close to weld metal; HAZ of S355J2 consists in ferritic-pearlitic matrix.

Table 2. Specimens' geometry and preparation.

Type of joint & PT results	Macrograph & HBW position HAZ ADI 1050 & HAZ S355J2 micrographs
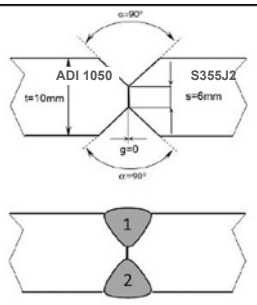 A) partial-penetration butt joint	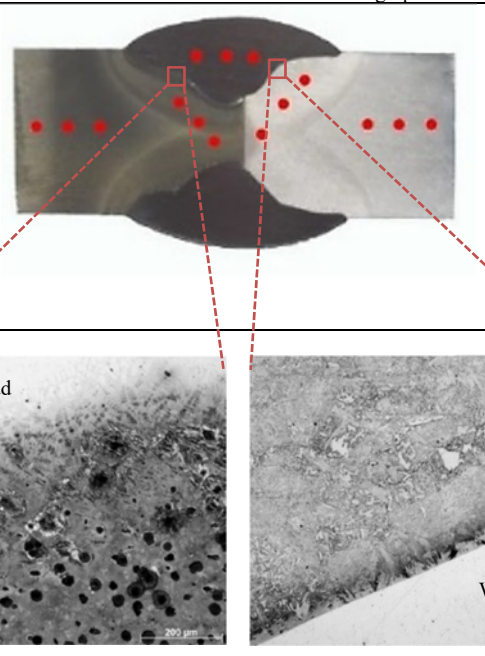
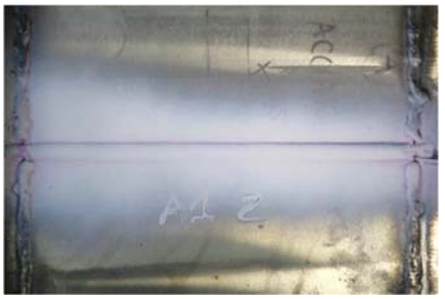	
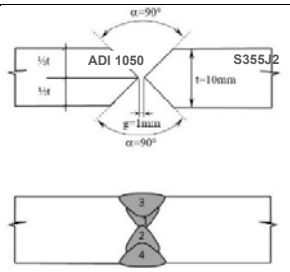 B1) full penetration butt joints B2) full penetration ground butt joints	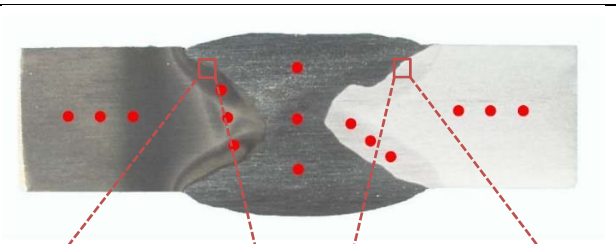
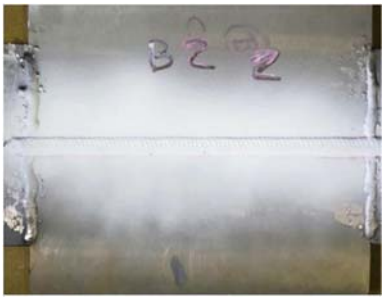	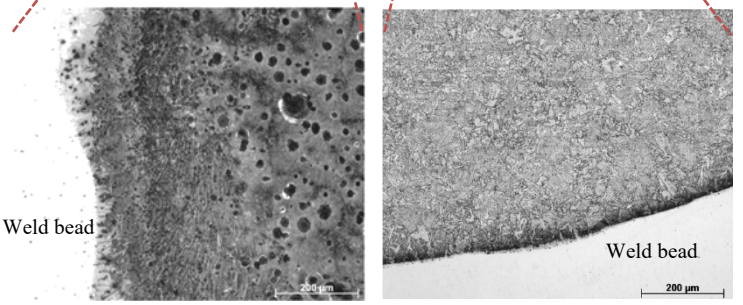

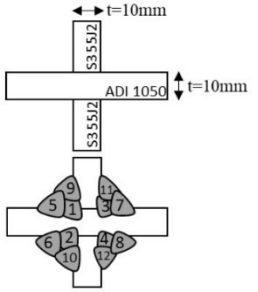

C) cruciform nlc fillet-welded joints

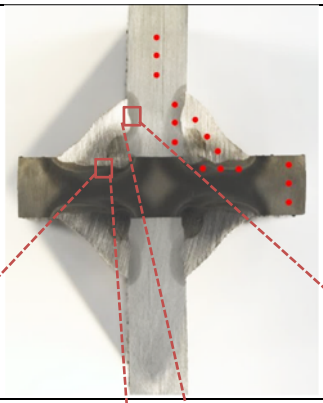

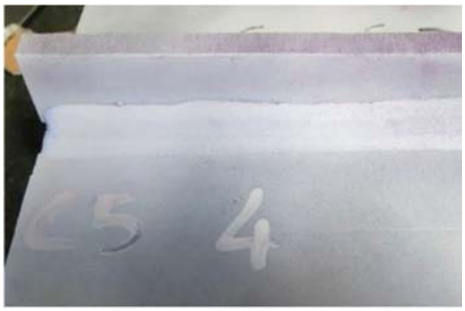

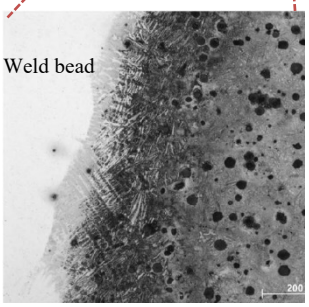

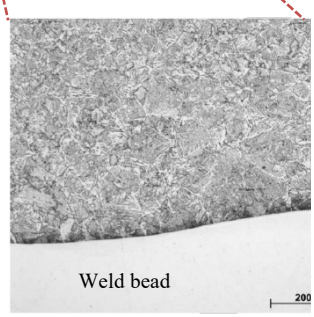

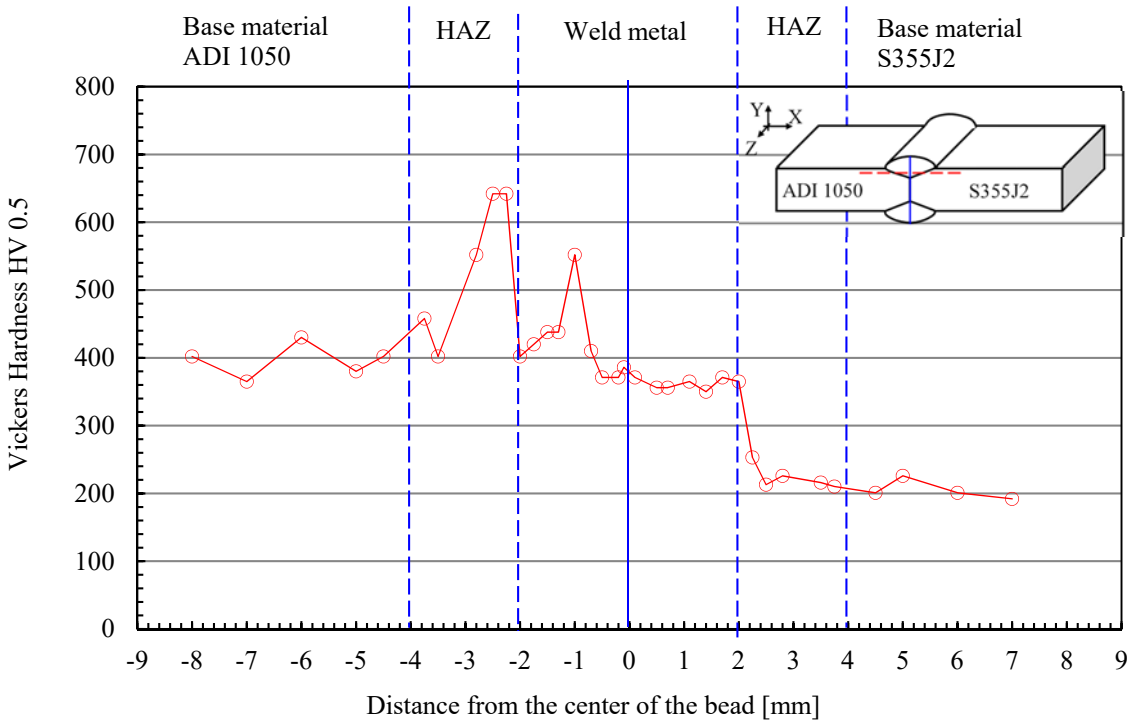

Fig. 2. HV0.5 measurement on cross section of a joint type A (partial-penetration butt-joint).

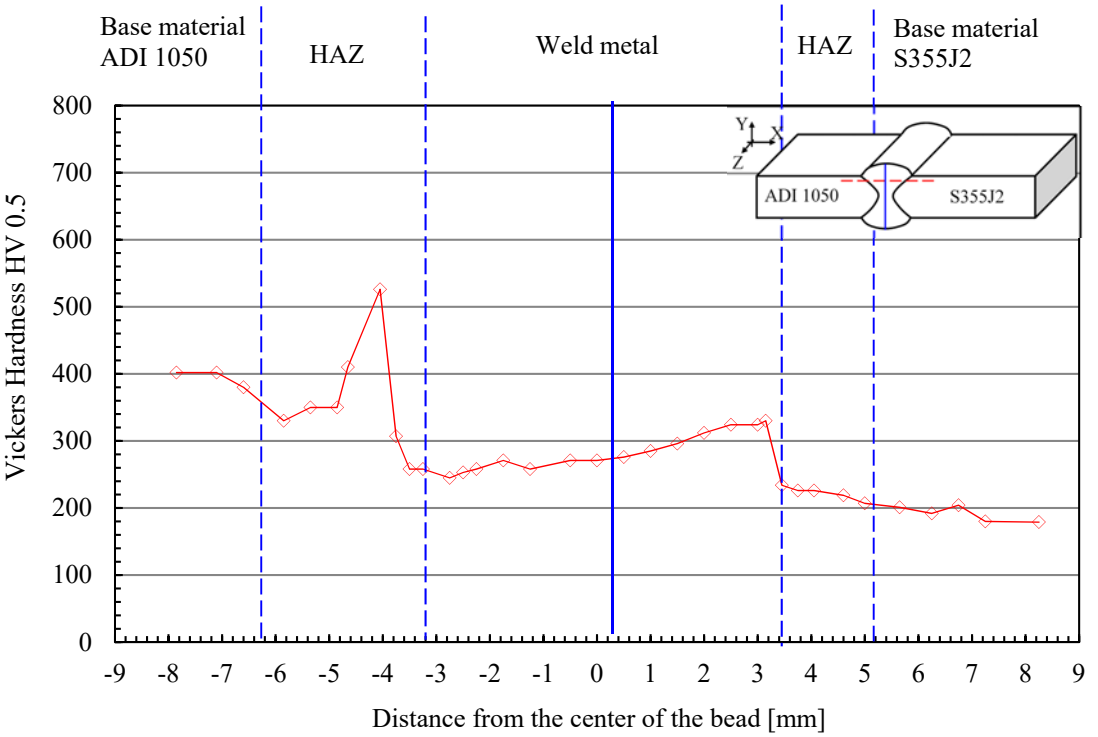

Fig. 3. HV0.5 measurement on cross section of a joint type B1 (full-penetration butt joint).

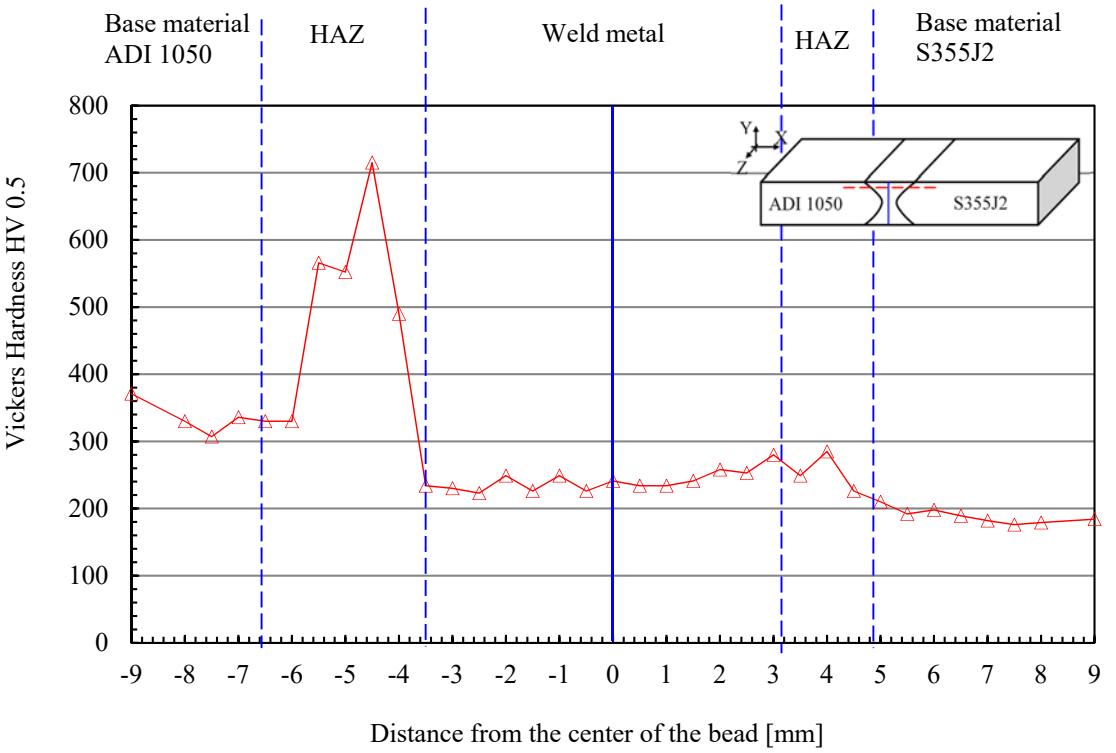

Fig. 4. HV0.5 measurement on cross section of a joint type B2 (full-penetration ground butt-joint).

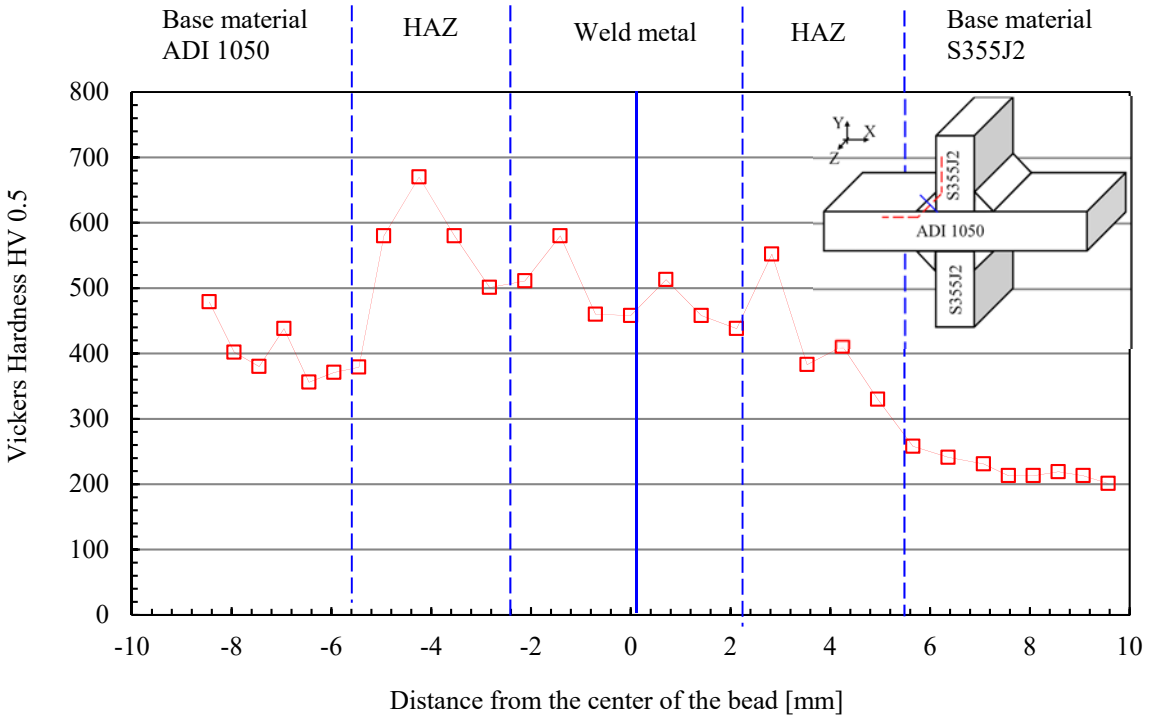

Fig. 5. HV0.5 measurement on cross section of a joint type C (cruciform nlc fillet-welded joint)

5. Fatigue tests

5.1 Testing parameters

Experimental fatigue tests were performed on welded joints presented in previous Figure 1, while Table 3 summarises the testing conditions and results. On the basis of the measured misalignments (Meneghetti et al. (2019)), which have not been reported here for sake of brevity, the fatigue loads were applied to each test series as follows:

- series A, partial-penetration butt-joints (Fig. 1a) were fatigue tested under axial loading to assess weld root as well as weld toe failure, after having milled the clamping surfaces to minimize the misalignments and reduce secondary bending effects;
- series B1, full-penetration butt-joints (Fig. 1b) were tested under four-point bending loading, in order to avoid secondary bending effects;
- series B2, full-penetration ground butt-joints (Fig. 1c) were fatigue tested under axial loading, as misalignments had been previously removed by milling the specimen surfaces to remove the weld caps;
- series C, cruciform nlc fillet-welded joints (Fig. 1d) were fatigue tested under four-point bending loading, in order to avoid secondary bending effects.

The experimental fatigue tests were carried out in standard laboratory environment by adopting a MFL axial servo-hydraulic machine, having a load capacity of 250 kN and equipped with a MTS TestStar IIm digital controller. The experimental fatigue tests were performed under closed-loop load control by imposing a constant amplitude sinusoidal load cycle with a nominal load ratio R as reported in Table 3. The load frequency was set in the range 10÷30 Hz depending on the applied load level. Fatigue failure of each specimen was defined as the number of loading cycles N_f at complete separation, while run-out has been fixed at $2 \cdot 10^6$ cycles, if no failure was detected.

Table 3. Testing conditions of the welded joints and summary of test results.

Specimen code	Joint detail	Testing condition*	tested specimens	Load#	Nominal load ratio R	failure criterion	$\Delta\sigma_A^*$ [MPa]	k	T_σ
A	Partial-penetration butt joints	AW	11	Ax	0.05	complete separation	73	4.88	1.91
B1	Full-penetration butt joints	AW	14	4PB	0.05	complete separation	139	4.42	1.91
B2	Full-penetration ground butt-joints	AW	6	Ax	0.05	complete separation	228	27.90	1.59
C	Cruciform nlc fillet-welded joints	AW	17 9	4PB	0.05 0.5	complete separation	132	6	2.8

* AW = as welded
# Ax=axial load, 4PB=four-point bending load

5.2 Damage analysis

Some examples of the fracture surfaces obtained after fatigue tests are reported in Figs. 6-9 for each test series.

Concerning partial-penetration butt-joints, multiple fatigue crack initiation locations were observed, as shown in the examples of Fig. 6. Fatigue cracks mainly initiated at the root side, then propagated through the weld throat. Additional propagating fatigue cracks were observed at the weld toe at the ADI side as well as at the interface between the ADI plate and the weld bead.

In the case of full-penetration butt-joints, the fatigue cracks always initiated at the weld toe at the ADI side as shown in Fig. 7, then propagated along the thickness of the joint. Only in one specimen, the fatigue crack initiated at the weld toe at the steel side.

Concerning full-penetration ground butt-joints, the fatigue cracks always initiated at the interface between the ADI plate and the weld bead as shown in Fig. 8, i.e. in the ledeburite region, then propagated along the thickness of the joint.

In the case of cruciform nlc fillet-welded joints, the fatigue cracks always initiated at the weld toe at the ADI side as shown in Fig. 9, then propagated along the thickness of the joint.

5.3 Fatigue results

The fatigue results are also reported in Figs. 10-13 in terms of number of cycles versus the applied nominal stress range $\Delta\sigma$ (defined as maximum value minus minimum value). It should be noted that in the case of partial-penetration butt-joints under axial loading, the nominal stress range $\Delta\sigma$ has been calculated in the weld throat area according to the following expression (see also Fig. 1a):

$$\Delta\sigma = \frac{\Delta F}{A_{throat}} = \frac{\Delta F}{W(t-2a)} \quad (1)$$

In the case of full-penetration ground butt-joints under axial loading, full-penetration butt-joints and cruciform nlc fillet-welded joints under four-point-bending loading, the nominal stress range has been calculated in the gross section.

The scatter bands reported in Figs. 10-13 are referred to survival probabilities of 2.3 and 97.7% and to a 95% confidence level. The endurable stress ranges at 2 million loading cycles for a survival probability 97.7%, the inverse slope k, and the scatter index T_σ are summarised in Table 3.

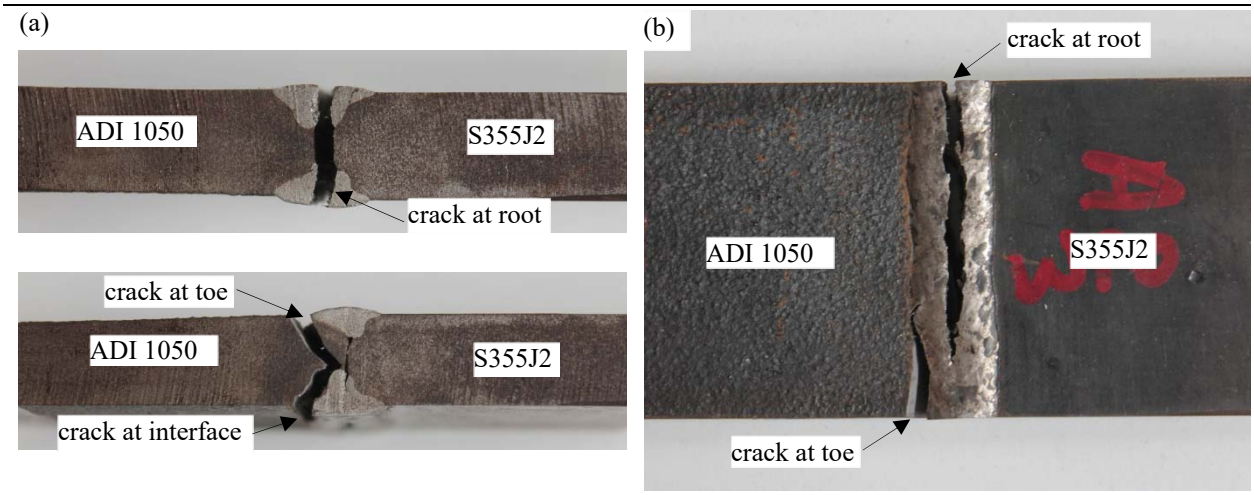

Specimen code: A2_3, AW, Axial loading, R= 0.05, $\Delta\sigma$ = 105.6 MPa, N_f = 1926134 cycles

Fig. 6. Fracture surfaces of partial-penetration butt-joints tested under axial fatigue loading.

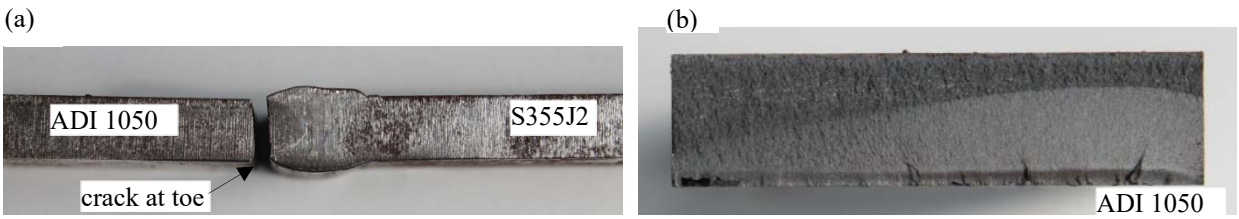

Specimen code: B5_3, AW, 4PB loading, R= 0.05, $\Delta\sigma$ = 261 MPa, N_f = 974888 cycles

Fig. 7. Fracture surfaces of full-penetration butt-joints tested under four-point-bending fatigue loading.

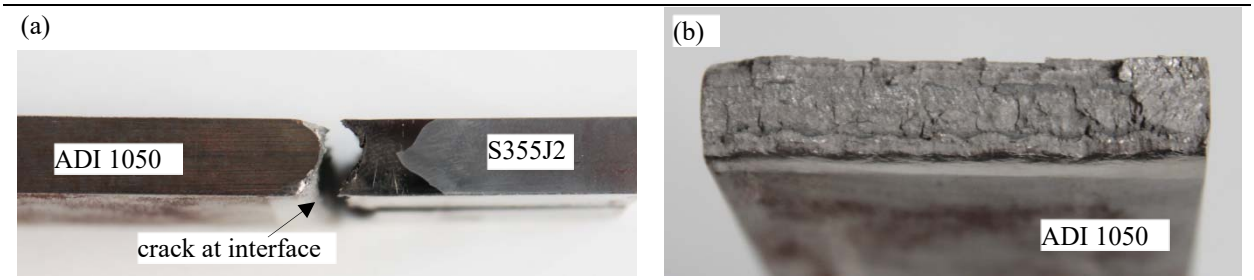

Specimen code: B4_2, AW, Axial loading, R= 0.05, $\Delta\sigma$ = 320 MPa, N_f = 109630 cycles

Fig. 8. Fracture surfaces of full-penetration ground butt-joints tested under axial fatigue loading.

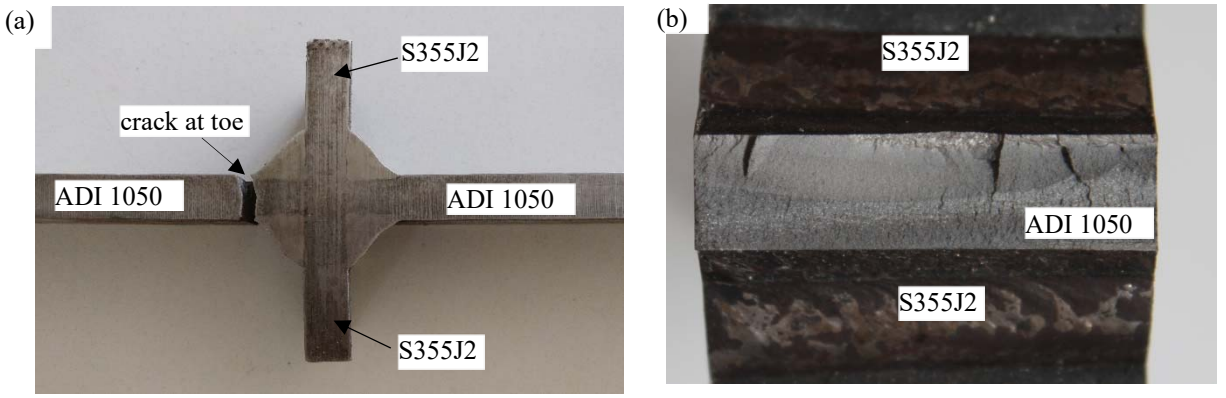

Specimen code: C11_1, AW, 4PB loading, R= 0.05, $\Delta\sigma$ = 322 MPa, N_f = 782127 cycles

Fig. 9. Fracture surfaces of cruciform nlc fillet-welded joints tested under four-point-bending fatigue loading.

Finally, Figs. 10-13 show that all tested welded details exhibit an endurable stress range, which is referred to a survival probability of 97.7% and 2 million loading cycles, higher than the FAT values suggested by Eurocode 3 and IIW Recommendations (Eurocode 3 (2005); Hobbacher (2016)) for corresponding homogeneous joints made of structural steels, especially at the medium-high cycle fatigue regime.

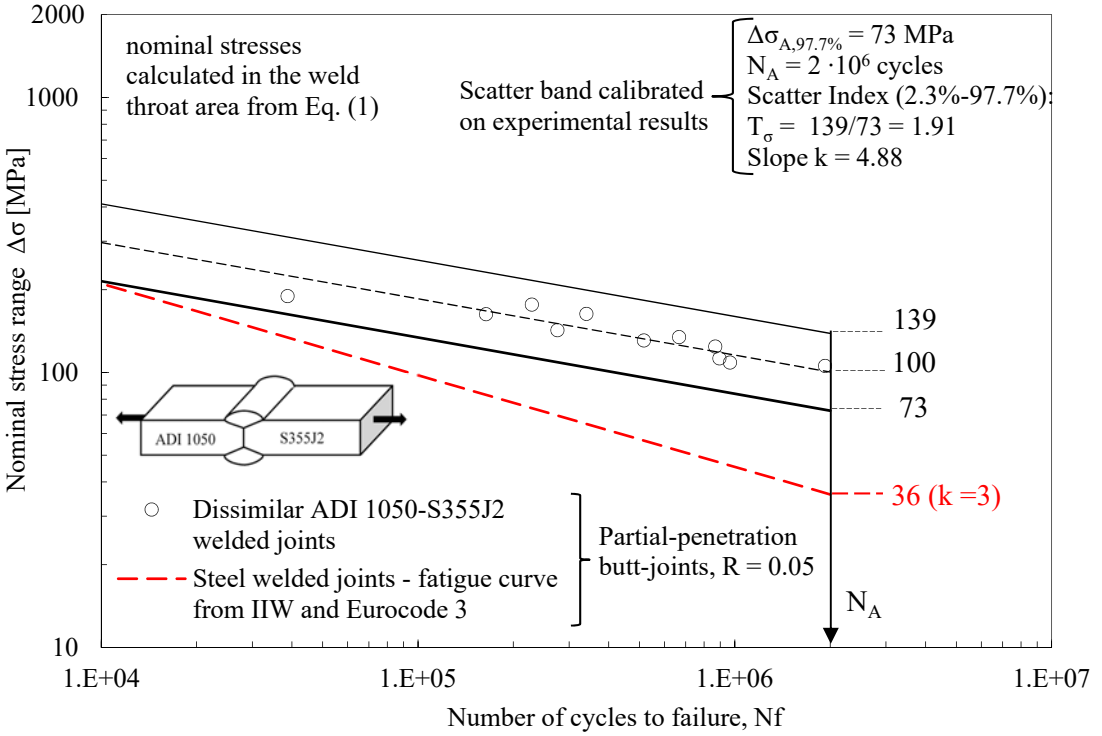

Fig. 10. Experimental results of axial fatigue tests performed on partial-penetration butt-joints; nominal axial stress range evaluated in the weld throat area.

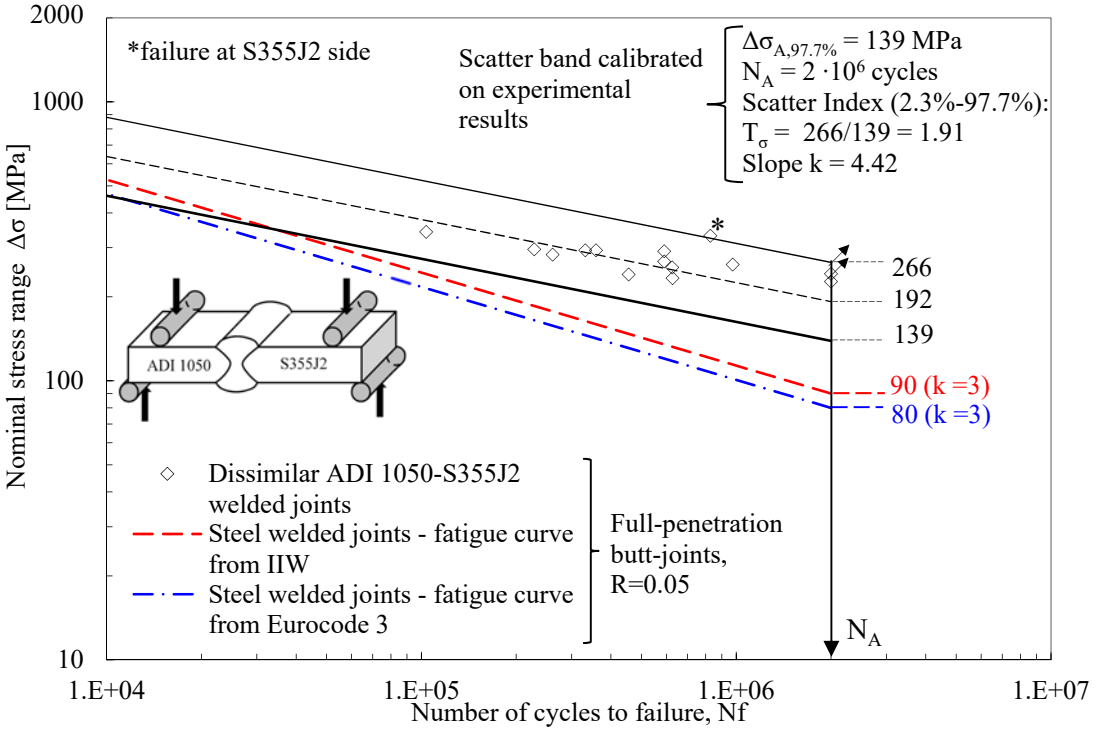

Fig. 11. Experimental results of four-point-bending fatigue tests performed on full-penetration butt-joints; nominal bending stress range evaluated in the cross-section area.

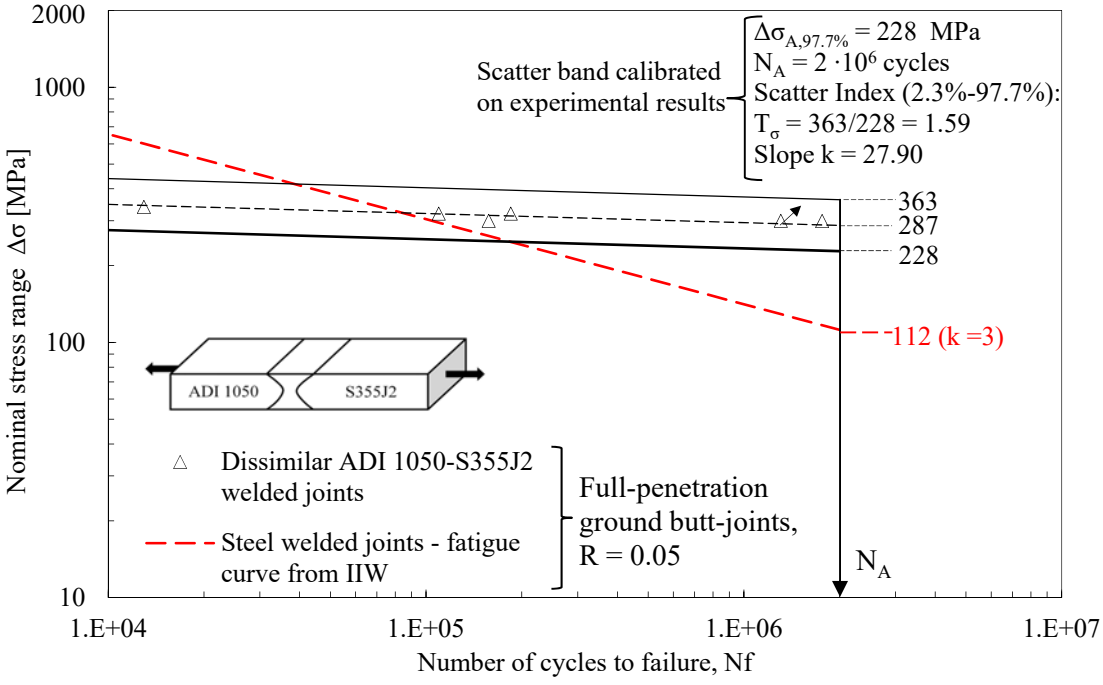

Fig. 12. Experimental results of pure axial fatigue tests performed on full-penetration ground butt-welded joints; nominal axial stress range evaluated in the cross-section area.

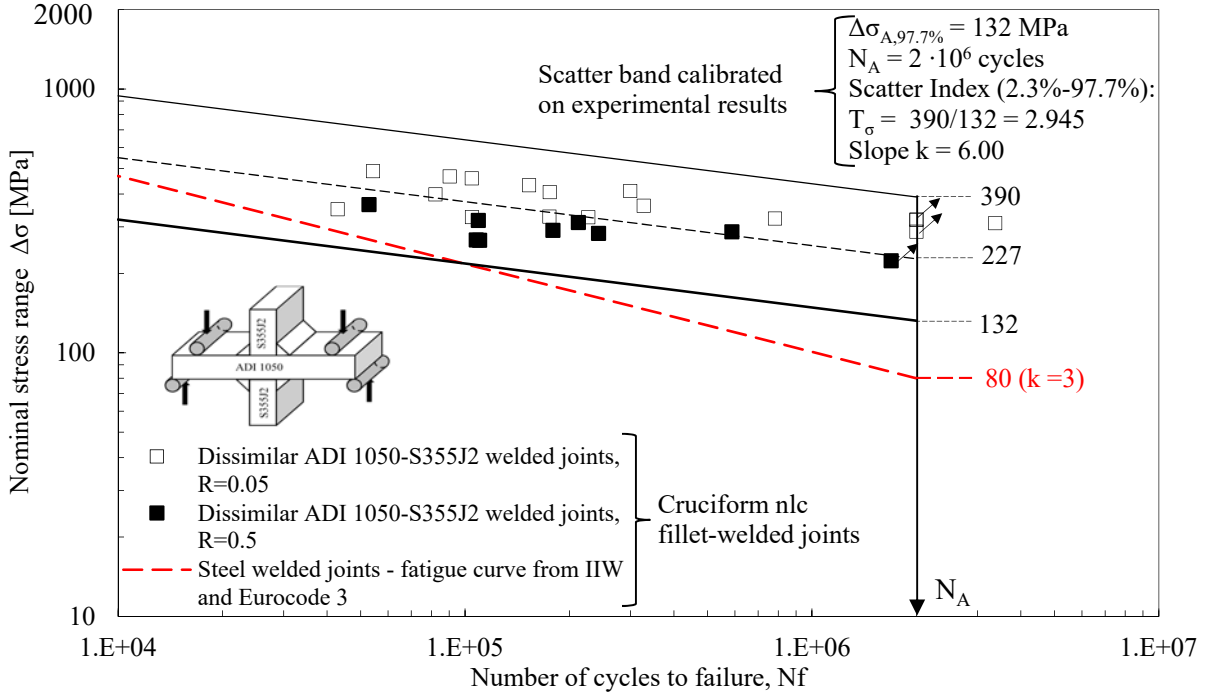

Fig. 13. Experimental results of four-point-bending fatigue tests performed on cruciform nlc fillet-welded joint; nominal bending stress range evaluated in the cross-section area. Experimental results obtained by adopting a nominal load ratio R= 0.05 and 0.5.

6. Conclusions

In the present contribution, the fatigue behavior of austempered ductile iron (EN-JS-1050)-to-steel (S355J2) dissimilar arc-welded joints has been experimentally investigated. The strength categories of some typical welded details were derived and compared with the categories provided by standards and recommendations for homogeneous steel welded joints. All joints were tested in the as-welded conditions. It was observed that the fatigue performances of austempered ductile iron-to-steel dissimilar arc-welded joints are better than those suggested by International Standards and Recommendations for the corresponding steel welded joints. Therefore, the fatigue strength assessment of ADI-to-steel dissimilar arc-welded joints could be performed on the safe side by applying the nominal stress approach proposed by International Standards and Recommendations for the corresponding steel welded joints. However, it is widely recognized in the literature that the best level of accuracy in the fatigue strength assessment of a welded structure can be obtained from local approaches (Radaj and Vormwald (2013)). Thus, the application of local approaches to dissimilar welded joints by taking into account the different material regions, where the fatigue crack initiates and propagates, should be considered and developed for future research.

References

Al Zamzami, I., Davison, B., Susmel, L., 2019. Nominal and local stress quantities to design aluminium-to-steel thin welded joints against fatigue. Int J Fatigue 123:279–295.

Bettahar, K., Bouabdallah, M., Badji, R., et al., 2015. Microstructure and mechanical behavior in dissimilar 13Cr/2205 stainless steel welded pipes. Mater Des 85:221–229.

Eslami, N., Harms, A., Henke, B., et al., 2019. Electrical and mechanical properties of friction stir welded Al-Cu butt joints. Weld World 63:903–911.

Eurocode 3: Design of steel structures – part 1–9: Fatigue, CEN, 2005

Eurocode 9: Design of aluminium structures - Part 1-3: Structures susceptible to fatigue, CEN, 2011

Figner, G., Vallant, R., Weinberger, T., et al., 2009. Friction Stir Spot Welds between Aluminium and Steel Automotive Sheets:

Influence of Welding Parameters on Mechanical Properties and Microstructure. Weld World 53:R13–R23.
Geng, H., Sun, L., Li, G., et al., 2019. Fatigue fracture properties of magnetic pulse welded dissimilar Al-Fe lap joints. Int J Fatigue 121:146–154.
Hobbacher, A.F., 2016. Recommendations for Fatigue Design of Welded Joints and Components. IIW Collection. Springer International Publishing
Infante, V., Braga, D.F.O., Duarte, F., et al., 2016. Study of the fatigue behaviour of dissimilar aluminium joints produced by friction stir welding. Int J Fatigue 82:310–316.
Katayama, S., 2004. Laser welding of aluminium alloys and dissimilar metals. Weld Int 18:618–625.
Kumar, S., Singh, P.K., Karn, K.N., Bhasin, V., 2017. Experimental investigation of local tensile and fracture resistance behaviour of dissimilar metal weld joint: SA508 Gr.3 Cl.1 and SA312 Type 304LN. Fatigue Fract Eng Mater Struct 40:190–206.
Martinsen, K., Hu, S.J., Carlson, B.E., 2015. Joining of dissimilar materials. CIRP Ann 64:679–699.
Meneghetti, G., Campagnolo, A., Berto, D., et al., 2019, Fatigue properties of austempered ductile iron-to-steel dissimilar arc-welded joints. In: IIW Annual assembly. IIW Doc. XIII-2786-19. Bratislava (Slovakia),
Mohammadzadeh, P. S., Häfele, P., Rethmeier, M., Schmid, A., 2015. Study on fatigue behavior of dissimilar materials and different methods of friction-welded joints for drive pinion in trucks. Weld World 59:917–926.
Okamura, H., Aota, K., 2004. Joining of dissimilar materials with friction stir welding. Weld Int 18:852–860.
Parkes, D., Xu, W., Westerbaan, D., et al., 2013. Microstructure and fatigue properties of fiber laser welded dissimilar joints between high strength low alloy and dual-phase steels. Mater Des 51:665–675.
Paventhan, R., Lakshminarayanan, P.R., Balasubramanian, V., 2011. Fatigue behaviour of friction welded medium carbon steel and austenitic stainless steel dissimilar joints. Mater Des 32:1888–1894.
Radaj, D., Vormwald, M., 2013. Advanced Methods of Fatigue Assessment. Springer Berlin Heidelberg, Berlin, Heidelberg
Rao, H.M., Kang, J., Shi, L., et al., 2018. Effect of specimen configuration on fatigue properties of dissimilar aluminum to steel resistance spot welds. Int J Fatigue 116:13–21.
Roberts, D.I., Ryder, R.H., Viswanathan, R., 1985. Performance of Dissimilar Welds in Service. J Press Vessel Technol 107:247.
Sun, M., Behravesh, S.B., Wu, L., et al., 2017. Fatigue behaviour of dissimilar Al 5052 and Mg AZ31 resistance spot welds with Sn-coated steel interlayer. Fatigue Fract Eng Mater Struct 40:1048–1058.
Taban, E., Gould, J.E., Lippold, J.C., 2010. Dissimilar friction welding of 6061-T6 aluminum and AISI 1018 steel: Properties and microstructural characterization. Mater Des 31:2305–2311.
Uzun, H., Dalle Donne, C., Argagnotto, A., et al., 2005. Friction stir welding of dissimilar Al 6013-T4 To X5CrNi18-10 stainless steel. Mater Des 26:41–46.
Zhang, Q., Zhang, J., Zhao, P., et al., 2016. Low-cycle fatigue behaviors of a new type of 10% Cr martensitic steel and welded joint with Ni-based weld metal. Int J Fatigue 88:78–87.
Zhang, W.C., Zhu, M.L., Wang, K., Xuan, F.Z., 2018a. Failure mechanisms and design of dissimilar welds of 9%Cr and CrMoV steels up to very high cycle fatigue regime. Int J Fatigue 113:367–376.
Zhang, W., Jiang, W., Zhao, X., Tu, S.T., 2018b. Fatigue life of a dissimilar welded joint considering the weld residual stress: Experimental and finite element simulation. Int J Fatigue 109:182–190.